Simulation of Indian summer monsoon intraseasonal oscillations in a superparameterized coupled climate model: need to improve the embedded cloud resolving model

**Bidyut B. Goswami · P. Mukhopadhyay ·
Marat Khairoutdinov · B. N. Goswami**

Abstract The characteristic features of Indian summer monsoon (ISM) and monsoon intraseasonal oscillations (MISO) are analyzed in the 25 year simulation by the superparameterized Community Climate System Model (SP-CCSM). The observations indicate the low frequency oscillation with a period of 30–60 day to have the highest power with a dominant northward propagation, while the faster mode of MISO with a period of 10–20 day shows a stationary pattern with no northward propagation. SP-CCSM simulates two dominant quasi-periodic oscillations with periods 15–30 day and 40–70 day indicating a systematic low frequency bias in simulating the observed modes. Further, contrary to the observation, the SP-CCSM 15–30 day mode has a significant northward propagation; while the 40–70 day mode does not show prominent northward propagation. The inability of the SP-CCSM to reproduce the observed modes correctly is shown to be linked with inability of the cloud resolving model (CRM) to reproduce the characteristic heating associated with the barotropic and baroclinic vertical structures of the high-frequency and the low-frequency modes. It appears that the superparameterization in the General Circulation Model (GCM) certainly improves seasonal mean model bias significantly. There is a need to improve the CRM through which the barotropic and baroclinic modes are simulated with proper space and time distribution.

1 Introduction

The systematic errors of global climate models arising from the uncertainties in the cloud parameterizations are well documented (Randall et al. 2007; Guilyardi et al. 2009). However, recent study by Stan et al. (2010) shows promise in capturing the climate variability on intraseasonal timescale using a Multi-scale Modelling Framework (MMF) through superparameterized Community Climate System Model (SP-CCSM). Due to the success of SP-CCSM in realistically capturing the ENSO variability and Madden-Julien Oscillations (MJO), they argued that superparameterization approach could play a key role in improving the intraseasonal variability of the climate model simulation. In another recent study, DeMott et al. (2011) demonstrated better capabilities of SP-CCSM in capturing the convectively coupled equatorial waves due to better oceanic response through ocean coupling in the SP-CCSM. Motivated by these two research works, we take up the present study to evaluate the model simulation of Indian summer monsoon (ISM) and monsoon intraseasonal oscillations (MISO) which will bring out the strength and weaknesses of the superparameterized framework for simulating ISM and MISO. SP-CCSM being a fully coupled model, we would like to see the impact of air-sea coupling on the simulation of MISOs as well, which was missing in our earlier study on MISO based on superparameterized Community Atmospheric Model version-2 (SP-CAM) simulation (Goswami et al. 2011; G1 hereon).

In G1, it was shown that, SP-CAM had a reasonable mean ISM rainfall, but it had a significant wet bias during northern summer over the Asian monsoon region, owing to

B. B. Goswami · P. Mukhopadhyay (✉) · B. N. Goswami
Indian Institute of Tropical Meteorology,
Dr. Homi Bhabha Road, Pashan, Pune 411008, India
e-mail: parthasarathi64@gmail.com

M. Khairoutdinov
School of Marine and Atmospheric Science,
New York University, Stony Brook, NY, USA

higher frequency of occurrence of rain events. Also, the model showed limited ability to capture observed intra-seasonal modes and their variabilities. Finally, G1 identified the vertical structure of convective heating tendencies simulated by the CRM to be one of the key reasons behind these biases. Our intention is to find whether the skill of SP-CCSM as it is discussed in DeMott et al. (2011) and Stan et al. (2010) remains equally valid for the simulation of ISM and different modes of MISO. As simulating the MISO remains one of the major challenges of the global climate models (Waliser et al. 2003; Lin et al. 2008), this study will provide insight toward "*whether a superparameterized coupled climate model captures the ISM and its different phases with fidelity*". We also would like to provide insight on the possible role of the CRM heating tendencies in the bias of SP-CCSM in simulating ISM and MISO as well. The model description and methodology is described in sect. 2 followed by results and discussion in sect. 3 and conclusion in sect. 4.

2 Model description, data used and methodology

We have used the superparameterized (Grabowski 2001; Khairoutdinov and Randall 2001; Khairoutdinov et al. 2005) Community Climate System Model, version 3 (CCSM) (Collins et al. 2006) (SP-CCSM) 25 years output. The details about the SP-CCSM run and the 2-D embedded CRM is explained in detail in Stan et al. (2010). The physical processes such as convection and stratiform cloudiness are represented by the embedded CRM of 4 km horizontal resolution within each General Circulation Model (GCM) grid and provide the CRM feedback to the GCM at the end of each GCM time step. The strength of the MMF approach is that even though a GCM is not being run at cloud resolving scale globally, it is able to incorporate the sub-grid scale processes with better representation.

Various observations and reanalysis are used to evaluate the model simulation. Global scale precipitation estimates, provided by the Global Precipitation Climatology Project daily at $1° \times 1°$ (GPCP) resolution for 1998–2008 (Huffman et al. 2001), regridded using bilinear interpolation technique (in bilinear interpolation the unknown value is determined considering the closest 2×2 neighborhood of known grid point values, surrounding the unknown computed location) to model resolution $2.8° \times 2.8°$ is used as precipitation observation. The National Oceanic and Atmospheric Administration (NOAA) (Liebmann and Smith 1996) Outgoing Longwave Radiation (OLR) data set from 1986 to 2003 is used to provide additional diagnostics of convective variability. Horizontal winds are taken from the National Centers for Environmental Prediction (NCEP) reanalysis data (Kalnay et al. 1996).

In order to extract MISOs from the simulation and observations, daily anomalies are calculated as the departure of daily values from a smoothed climatology at daily resolution. The smoothed climatology is reconstructed based on the annual mean and first three harmonics of the long-term mean seasonal cycle. The techniques used for carrying out the analyses in the study are data filtering using Lanczos filter (Duchon 1979), Lag-regression analysis (Wilks 1995), Space–Time spectra (Wheeler and Kiladis 1999), and Hovmöller plots (Hovmoller 1949).

3 Results and discussion

3.1 Mean state

Before evaluating the skill of a model in simulating the Intra-seasonal Oscillations (ISO), we need to see how good the mean climate of the model is in the South Asian Monsoon region. In Fig. 1a, b we compare the model-simulated mean June–July–August–September (JJAS) rainfall and 850 hPa wind (Fig. 1c–d) with the corresponding observation. The amount of mean seasonal (JJAS) rainfall over the ISM domain (shown by the red box in Fig. 1a; 55–100°E, 10°S–30°N) for GPCP = 687.636 mm, SP-CAM = 822.612 mm, SP-CCSM = 618.176 mm. So the model SP-CCSM not only is reasonable with respect to observation over the land region but also shows a significant improvement in biases over the oceanic region as compared to its uncoupled Atmospheric GCM simulation by SP-CAM (see Fig. 2b of G1). However in spite of the improvement in SP-CCSM, the oceanic branch of the Tropical Convergence Zone (TCZ) is absent in the simulations (Fig. 1b) and the continental TCZ is too zonal compared to the observations. The 850 hPa JJAS mean wind is well reproduced by SP-CCSM as compared to the observed winds. It should be noted that, apart from the intensity, there is hardly any change in the pattern of the mean JJAS winds, compared to the SP-CAM simulation (see Fig. 2d of G1). However, in a few locations such as (53°E, 15°N), (78°E, 10°N) and (90°E, 20°N) the intensity of the mean JJAS 850 hPa wind shows notable improvement in SP-CCSM simulation (Fig. 1d) over that of the SP-CAM (see Fig. 2d of G1). We find that the remarkable improvement of SP-CCSM simulation of mean rainfall over that of SP-CAM lies in capturing the probability of occurrences of various rainfall categories. We analyzed the probability density of different rain rate categories over different regions namely the Central India (CI), Bay of Bengal (BoB), Arabian Sea (AS) and Equatorial Indian Ocean (EqIO). Like many GCMs (Piani et al. 2010), our earlier result on SP-CAM (G1) shows significant problem in capturing the probability distribution function (PDF) of rain rate in general and the
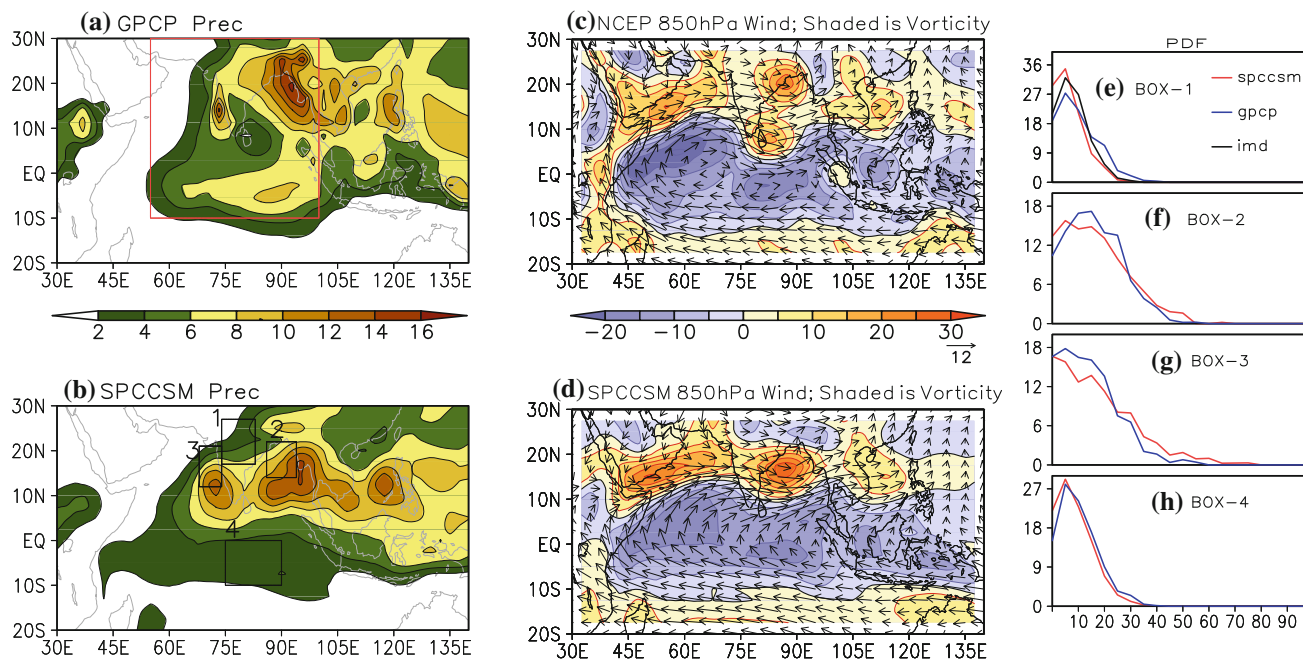
Fig. 1 Climatological mean (JJAS) precipitation (mm d^{-1}) from **a** GPCP and **b** SP-CCSM and 850 hPa winds (ms^{-1}) from **c** NCEP and **d** SP-CCSM. In Fig. 1c–d, in *shading* is the corresponding vorticity (10^{-6} s^{-1}). RHS panels show, Probability distribution function for representative boxes over **e** Central India (BOX-1), **f** Bay of Bengal (BOX-2), **g** Arabian Sea (BOX-3) and **f** Equatorial Indian Ocean (BOX-4) (the boxes are shown in Fig. 1b), based on daily rainfall (mm d^{-1}) with a bin width of 5 mm. [For Fig. 1e–h; different rainfall classes (mm/day) along x-axis, and percentage of total rainfall along y-axis]

lighter rain rate in particular. However, Fig. 1e–h shows that SP-CCSM simulates the frequency distribution of observed rain rates quite well. It is also of considerable interest that even the PDF of lighter rain rate has been significantly improved.

3.2 MISOs

In Fig. 2a–b the simulated Intra-seasonal Variability (ISV), defined as the standard deviation of the 10–90 day band-pass filtered (Duchon 1979) daily precipitation anomaly during JJAS is compared with the observation. The ISV simulated by the model (Fig. 2a) is reasonably well correlated (over the area 6.5–38.5°N and 66.5–100.5°E) with the observed ISV pattern (Fig. 2b). Also the similarity between the spatial patterns of the ISV and the climatological seasonal mean rainfall suggest that the model rainfall follows a Poisson distribution, much similar to the observations. The simulation of the rainfall distribution is also evident from Fig. 1e–h.

Figure 2c–f shows the East–West and North–South space–time spectra highlighting the dominant modes of oscillations in the daily precipitation field from GPCP and SP-CCSM computed following the methodology of Wheeler and Kiladis (1999). We have computed the signal-to-noise-ratio (SNR) of precipitation by dividing the raw power in precipitation by an estimate of its red noise

background. The red noise background is estimated by passing a 1–2–1 filter through the power repeatedly in both wavenumber and frequency, till the filter saturates. Figure 2c–d shows the zonally propagating modes for global data with the resulting SNR of precipitation being averaged between 15°S and 15°N, for SP-CCSM output and observed data (GPCP), respectively. Similarly, Fig. 2e–f shows the meridionally propagating modes over the ISM domain (between 20°S and 30°N) with the SNR of precipitation being averaged between 65°E and 100°E, for SP-CCSM output and observed data (GPCP), respectively. It should be noted that for the Fig. 2e, f, wavenumber 1 corresponds to the largest wave that exactly fits inside the latitude band 20°S–30°N. Also, it should be kept in mind that due to non-periodic domain some artificial spectral power may get introduced into the meridional space–time spectrum (Fig. 2e, f). However, sensitivity tests (viz., different smoothening, slight change in the domain size, etc.) indicate that the location and strength of the dominant spectral signals remains fixed.

Comparison of Fig. 2c, d reveals, while the observation has a 30–60 day eastward propagating mode with wavenumber 1, the model simulates an eastward propagating mode with periodicity of 40–70 day and wavenumber 1. There is also a westward propagating mode of 10–20 day periodicity and wavenumber 5 in the observation (Fig. 2d). In contrast, the model simulates a westward propagating
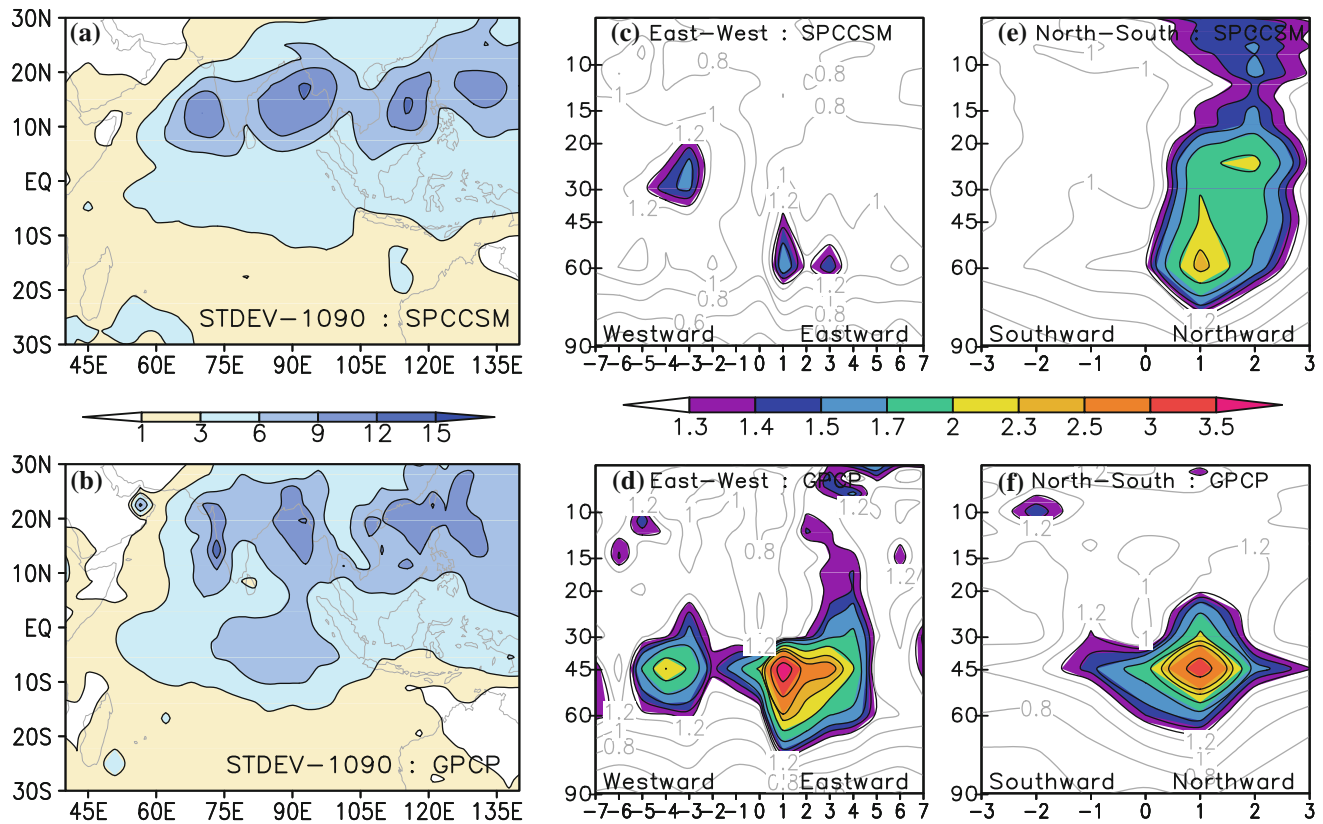
Fig. 2 Standard deviation (STDEV) of 10–90 day bandpass filtered daily precipitation (mm day^{-1}) anomalies (JJAS) from **a** SP-CCSM and **b** GPCP. Zonal wave number frequency spectra of precipitation (divided by the background spectrum) calculated over global tropics (15S–15N) for **c** SP-CCSM and **d** GPCP. Meridional wave-number frequency spectra of precipitation (divided by the background spectrum) calculated over 20S–30N, 60E–100E for **e** SP-CCSM and **f** GPCP. [Note for Fig. 2e–f, wavenumber 1 corresponds to the largest wave that exactly fits into 50 latitudes, from 20 S to 30 N]. All the wavenumber frequency spectra are *plotted* for JJAS

mode of periodicity 15–30 day and wavenumber 4 (Fig. 2c). In the meridional direction, a dominant north-ward propagating mode of periodicity 30–60 day and wavenumber 1 is found (Fig. 2f) in the observation. On the other hand the model simulates (Fig. 2e) a northward propagating mode with 40–70 day periodicity and wave-number 1. Comparing Fig. 2f with 2e the northward propagation in 40–70 day mode with wavenumber 1 is found to be relatively weak in SP-CCSM simulation. Rather the high frequency mode with period 15–30 day and wavenumber 2 shows a prominent northward propa-gation (please note the secondary maximum in Fig. 2e).

Nevertheless, it should be noted that, compared to the SP-CAM simulation (see, Fig. 2b, d of G1) the SP-CCSM shows more realistic space–time distribution of precipita-tion; especially in the meridional direction. Both the SP-CAM (Fig. 2b of G1) and SP-CCSM (Fig. 2c) simulate an eastward propagating mode at wave number 1 with a longer period (40–70 day) than in the observations (30–60 day) (Fig. 2d). However, in the north–south direc-tion, SP-CAM simulates the dominant northward propa-gating mode with periodicity 15–30 day and wavenumber

1–2 (Fig. 2d of G1). In addition to having a meridional structure with wave number 1, the SP-CAM simulated 40–70 day mode, also has a significant meridional mean component (Fig. 2d of G1). Thus, in SP-CAM simulation, the dominant northward propagation is seen in the mode with periodicity 15–30 day and wavenumber 1–2 (Fig. 2d of G1). On the other hand, in the SP-CCSM simulations, the dominant northward propagation is seen in the mode with periodicity 40–70 day and wavenumber 1 (Fig. 2e). Therefore, compared to the observation where northward propagation is seen only in the slowly varying mode (30–60 day and wavenumber 1, Fig. 2f), space–time dis-tribution of precipitation in SP-CCSM stands better and improved over that of SP-CAM.

In summary, in observation we see three prominent ISO modes; one, an eastward propagating mode with a peri-odicity of 30–60 day and wavenumber 1 (Fig. 2d), which is the MJO; two, a westward propagating mode of periodicity 10–20 day and wavenumber 5 (Fig. 2d); and three, a northward propagating mode of periodicity 30–60 day and wavenumber 1 (Fig. 2f). The modes with 10–20 day peri-odicity and wavenumber 5 (Fig. 2d) and 30–60 day

periodicity and wavenumber 1 (Fig. 2f) are well documented to be the components of monsoon ISV (Goswami 2005).

The model-simulated eastward propagating component of the mode with 40–70 day periodicity and wavenumber 1 corresponds to the observed MJO signal (DeMott et al. 2011). The model simulates a westward and northward propagating 15–30 day mode with wavenumber 4 (Fig. 2c) and wavenumber 2 (Fig. 2e), and a northward propagating mode with periodicity 40–70 day and wavenumber 1 (Fig. 2e). We believe that the northward propagating 15–30 day mode (Fig. 2e) is actually a separate mode rather than being a part of a broadly defined northward propagating 40–70 day mode (Fig. 2e), based on the evidence that the model distinctively produces a mode with periodicity 15–30 day and wavenumber 4 (Fig. 2c) and wavenumber 2 (Fig. 2e).

For the ease of documentation of the simulation of the ISM ISO modes we here denote, the model-simulated westward and northward propagating mode of 15–30 day periodicity and wave-number 4 (Fig. 2c) and wavenumber 2 (Fig. 2e) as MISO-M1; the westward propagating observed mode of periodicity 10–20 day and wave-number 5 (Fig. 2c) as MISO-O1; the northward propagating model-simulated mode of periodicity 40–70 day and wave-number 1 mode (Fig. 2e) as MISO-M2; the northward propagating observed mode of periodicity 30–60 day and wave-number 1 (Fig. 2f) as MISO-O2. So, the question that arises is whether the modes MISO-M1 and MISO-M2 are the model-simulated counterparts for the observed modes MISO-O1 and MISO-O2?

3.3 Analyzing ISO modes

To isolate and then analyze the model-simulated modes MISO-M1 and MISO-M2, we have applied 15–30 and 35–80 day Lanczos band-pass filter, respectively, on the model output. To compare with the observation, we have applied the 10–20 and 30–80 day Lanczos band-pass filter on the observation data and isolated the observed modes MISO-O1 and MISO-O2, respectively.

To identify the characteristics of simulated modes with that of the observations, the vertical cross section of composite of meridional wind anomaly for the two modes in peak active monsoon conditions is plotted (Fig. 3), averaged over the longitude band 70–90°E. Active monsoon conditions are based on an index defined as rainfall anomalies area averaged over the central India (72–83°E; 15–25°N) and standardized by its own standard deviation (Goswami et al. 2010; G1). We call it the central India precipitation index (CIPI). We have considered ISM as active when the CIPI value is above 1 for at least 3 consecutive days. The middle date of the active monsoon

period has been considered as the peak active date. This definition of peak active monsoon, suggests that the composite plots are of maximum relevance over the central Indian region. It appears (Fig. 3) that there is some improvement in the MISO-M1 and MISO-M2 simulation of SP-CCSM as compared to SP-CAM. However the difference between the meridional wind anomalies of the two MISO modes is not as distinct in SP-CCSM simulation (Fig. 3c, d) as in the observation (Fig. 3a, b). Rather, both the modes are simulated with similar features and with higher amplitude. The amplitudes of meridional wind anomalies are much stronger in SP-CAM simulation (Fig. 3e, f) than observation (Fig. 3a, b). Further, while for MISO-O1 mode the meridional wind anomalies are southerlies all the way up to 300 hPa (see around 12°N in Fig. 3a), in SP-CAM simulations they become northerlies at an altitude as low as 600 hPa. The SP-CCSM simulated meridional wind anomalies (Fig. 3c, d) look relatively improved compared to SP-CAM simulations. We notice from the Fig. 3g, h, the SP-CCSM-simulated vertical shear (*red line*) is stronger than what is observed (*black line*); and even stronger in SP-CAM-simulation (*blue line*). This gives an indication that although the mean is simulated well in SP-CCSM, the characteristic features of different modes have not been captured by the model realistically.

We further examined the propagation and structural features of the model-simulated modes, compared to the observed ones. We regressed the band-pass-filtered precipitation and wind anomalies of the respective modes, onto the CIPI, both for model-output and observation. The MISO-M1 mode is found to be westward propagating from the western Pacific, but becomes very slow in zonal direction over the Indian longitudes (Fig. 4a), and shows a northward propagation (Fig. 4b). The MISO-M1 mode partially shows a baroclinic character in the vertical structure (evident from the 200 and 850 hPa circulation pattern in Fig. 4c–d; also evident from strong vertical shear in Fig. 3c, g-*red line*). Contrary to MISO-M1 (Fig. 4a–d), the MISO-O1 mode has a westward propagating feature (Fig. 5a) and a dominantly barotropic vertical structure (Fig. 5c, d; also evident from Fig. 3a, g-*black line*).

The MISO-O2 mode is observed to propagate eastward over the longitudes 60–85°E and then becomes almost stationary (Fig. 5e) and northward from equator up to 25°N (Fig. 5f). The simulated MISO-M2 fails to show the rapid eastward movement over the Indian longitude belt; instead keeps on moving slowly up to east of the west pacific (150°E) (Fig. 4e). Further, along the meridional direction the simulated mode MISO-M2 shows a very feeble northward propagation, and looks almost stationary with the convection sitting over the latitude 16°N (Fig. 4f). However the simulated lower and upper level circulation pattern of MISO-M2 (Fig. 4g, h) resembles well with that
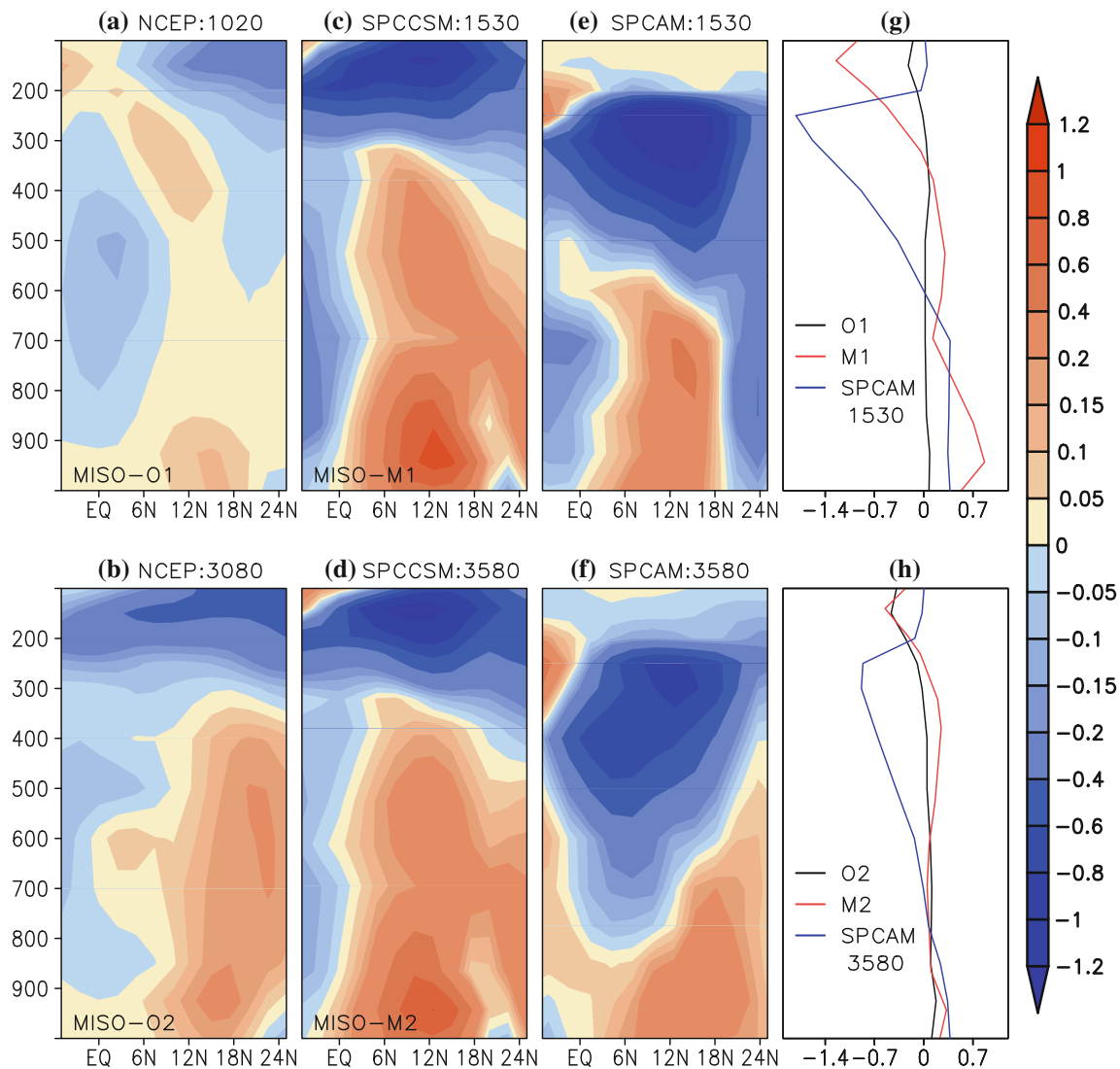
Fig. 3 Vertical cross section of peak active monsoon composite of meridional wind anomaly **a** NCEP: 10–20 day filtered, **b** NCEP: 30–80 day filtered, **c** SP-CCSM: 15–30 day filtered, **d** SP-CCSM: 35–80 day filtered, **e** SP-CAM: 15–30 day filtered, **f** SP-CAM: 35–80 day filtered; for the two MISO modes, averaged over the longitude band 70E–90E. **g** Peak active monsoon composite of meridional wind anomalies: NCEP: 10–20 day filtered (*black*), SP-CCSM: 15–30 day filtered (*red*), SP-CAM: 15–30 day filtered (*blue*); averaged over 10N–15N and 70E–90E. **h** Same as *panel* (**g**), except for NCEP: 30–80 day filtered (*black*), SP-CCSM: 35–80 day filtered (*red*), SP-CAM: 35–80 day filtered (*blue*)

of the observed mode MISO-O2 (Fig. 5g, h); although the simulated winds (Fig. 4g, h) are stronger than observed (Fig. 5g, h). These simulated upper and lower level circulation patterns (Fig. 4g, h) suggest that the model could capture the observed baroclinic vertical structure of the MISO-O2 (Fig. 5g, h, Fig. 3b) with some success.

3.4 Northward propagation of ISOs

From the evidences in hand, it is reasonable to consider that although the simulated MISO-M1 is close to the MISO-O1 mode on time scale, it exhibits quite different behavior and structure. In fact, the simulated MISO-M1

looks like a unique model generated new mode with no observational counterpart. MISO-M1 mode shows a northward propagation (Fig. 2e and Fig. 4b) and a considerable baroclinic vertical structure (Fig. 3c and Fig. 4c, d). The findings of G1 suggest that the SP-CAM also simulates a unique mode with periodicity 15–30 day and wavenumber 1–2 (Fig. 7d of G1) with no observational counterpart. This model-generated new mode mentioned in G1 shows prominent northward propagation and baroclinic vertical structure. G1 had concluded that the failure to realistically simulate the location of the low-level convergence relative to the convection maximum eventually led to the northward propagation of the model-generated new
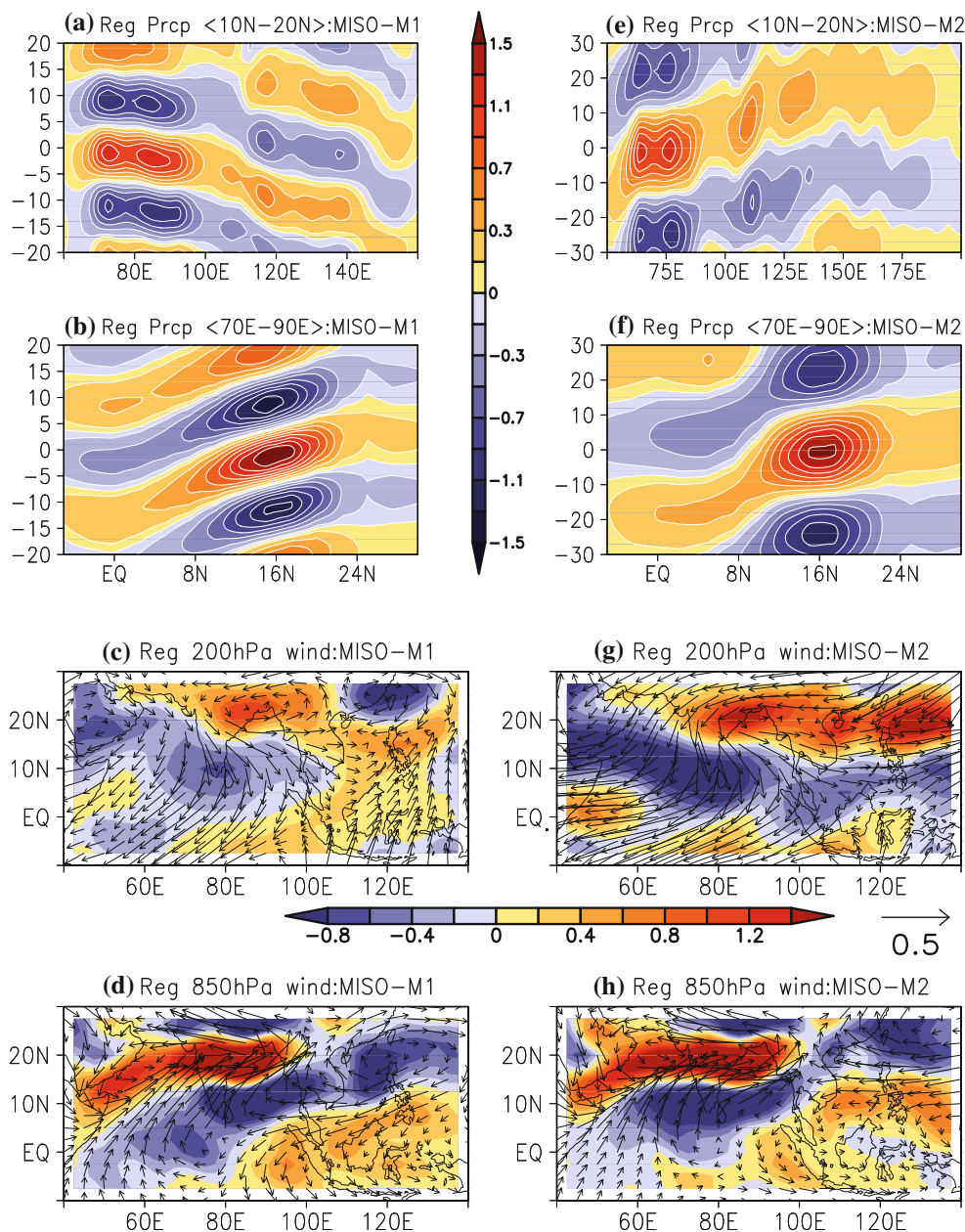
Fig. 4 a Longitude-time and **b** latitude-time *plots* of 15–30 day filtered SP-CCSM precipitation anomalies regressed on Central India Precipitation Index (CIPI), averaged over 10N–20N and 70E–90E, respectively. 15–30 day filtered SP-CCSM wind anomalies regressed on CIPI—**c** 200 hPa and **d** 850 hPa; in *shading* is the corresponding vorticity (10^{-6} s^{-1}). RHS *panels* are same as LHS *panels* but for 35–80 day filtered SP-CCSM wind

mode mentioned in G1. Jiang et al. (2004) showed that the observed northward propagation of the MISO results due to the low-level convergence positioned a few degrees north of the convection maximum. To explore the reason behind the northward propagation shown by the MISO-M1 mode, we also analyzed the simulation of the mechanism under the hypothesis proposed by Jiang et al. (2004) in the SP-CCSM output.

In Fig. 6 we have plotted the composite of barotropic and baroclinic components of vorticity anomaly, averaged

over 70–90°E, for the two modes in peak active monsoon conditions. The peak active monsoon condition has been defined in the same way as it had been done for Fig. 3. The bottom panels of Fig. 6 show the barotropic component of vorticity; while the top panels show the baroclinic component. In the bottom panels of Fig. 6, alongside barotropic component of vorticity, OLR composites are plotted for the respective MISO modes. Here barotropic component has been calculated by taking the column average of total vorticity; and baroclinic component has been computed
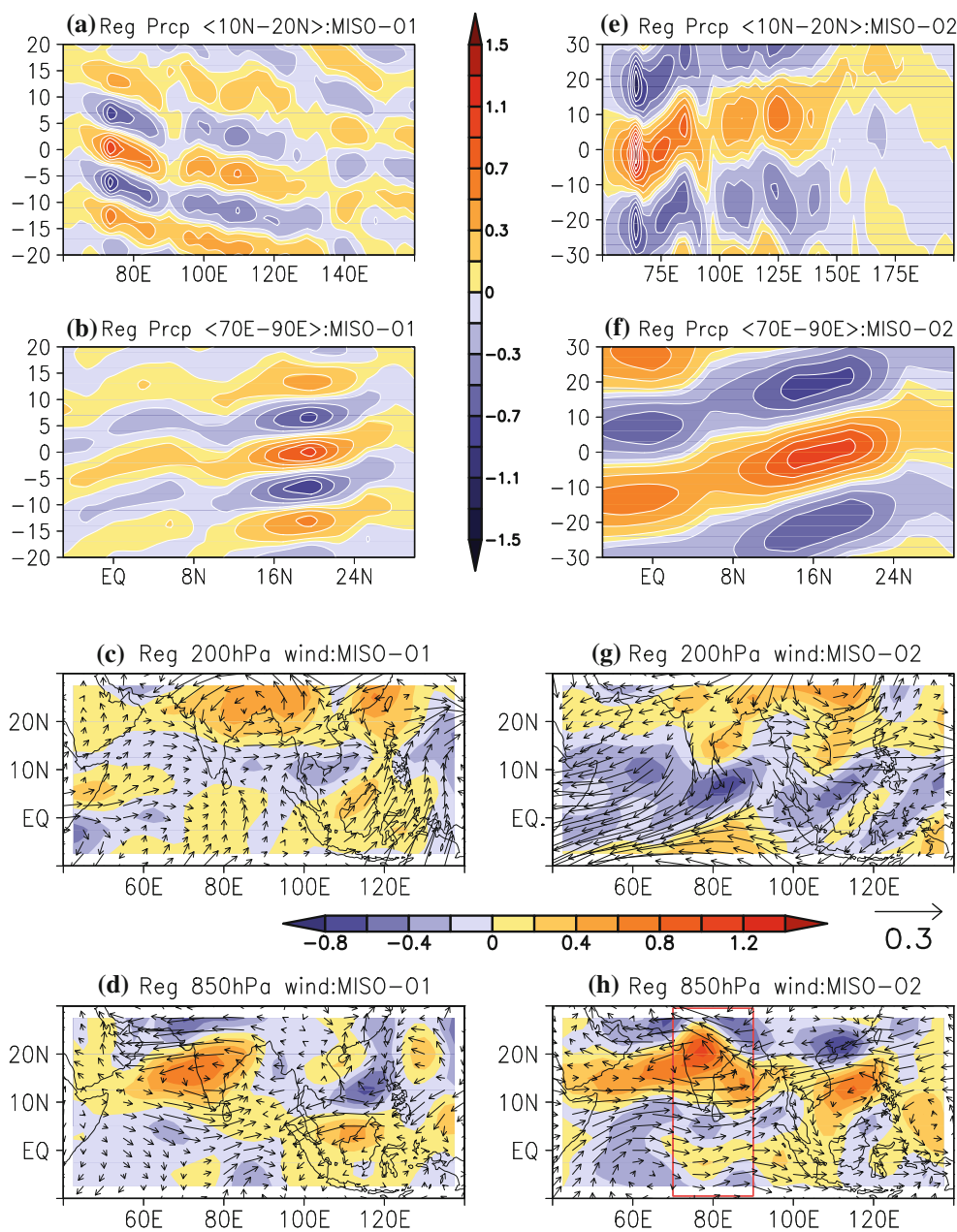
Fig. 5 a Longitude-time and **b** latitude-time *plots* of 10–20 day filtered GPCP precipitation anomalies regressed on Central India Precipitation Index (CIPI), averaged over 10N–20N and 70E–90E, respectively. 10–20 day filtered NCEP wind anomalies regressed on CIPI—**c** 200 hPa and **d** 850 hPa; in *shading* is the corresponding vorticity (10^{-6} s^{-1}). RHS *panels* are same as LHS panels but for 30–80 day filtered NCEP wind. The longitude band 70E–90E is *highlighted* in Fig. 5h, for ease of visualization of Figs. 3 and 6

subtracting this barotropic component from the total vorticity at each latitude and level. With the help of Fig. 6, we demonstrate that the model fails to simulate the two components of vorticity realistically. Consequently the low-level convergence, responsible for the northward propagation of the observed MISO modes, has not been simulated properly in the model. In fact, unlike the observation, the MISO-M1 mode shows a distinct northward propagation mainly due to its barotropic vorticity maxima lying to the north of the convection centre

(Fig. 6f). Whereas the MISO-M2 mode shows a weak northward propagation as its barotropic vorticity is found to be lagging behind the convection centre (Fig. 6h).

Heating is a key component in an atmospheric column in driving the convergence and divergence in the monsoon regime (Choudhury and Krishnan 2011); and consequently vorticity. As in the superparameterized framework, it is the embedded CRM which actually simulates the heating tendencies, we feel, the CRM heating tendencies could play an important role in the model bias. To find a possible source
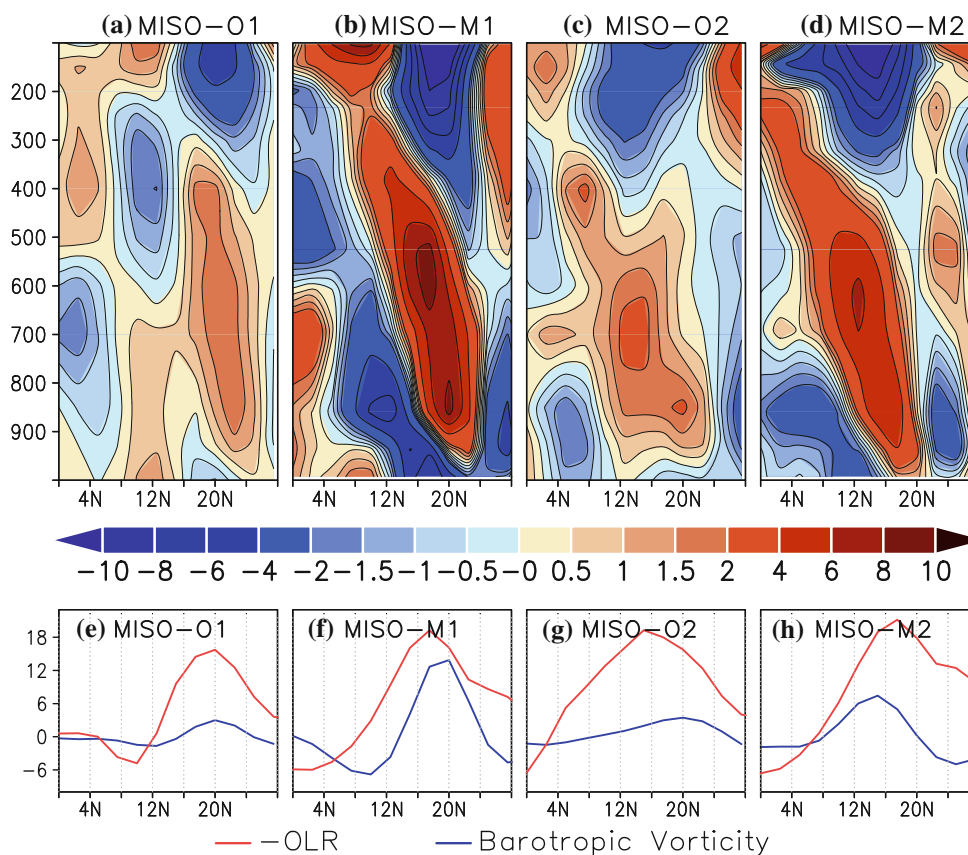
Fig. 6 Peak active monsoon composite of baroclinic component of vorticity (5×10^{-6} s^{-1}) anomaly averaged over 70E–90E: **a** NCEP: 10–20 day filtered, **b** SP-CCSM: 15–30 day filtered **c** NCEP: 30–80 day filtered, **d** SP-CCSM: 35–80 day filtered. Corresponding OLR (Wm^{-2}) (*red line*) and 850 hPa barotropic component of vorticity (*blue line*) (5×10^{-6} s^{-1}) composites are *plotted* at the *bottom panels* (**e**), (**f**), (**g**) and (**h**)

behind such model bias in capturing the high frequency and low frequency modes of MISO, we analyzed the CRM heating tendency over three selected regions. The peak active monsoon composite of heating tendencies for 15–30 and 40–70 day modes are shown in Fig. 7a–c. In Fig. 7d–f the peak active monsoon composites of the divergence profile are shown. Figure 7a–c shows that the simulated vertical heating patterns are identical for the two MISO modes. This leads to the same vertical structure of the two model-simulated modes, contrary to the observation where one MISO mode is barotropic (10–20 day mode) (Fig. 3a, Indian region in Figs. 5c–d, 6a) and the other one is baroclinic (30–60 day mode) (Fig. 3b, Indian region in Figs. 5g–h,6c) in the vertical. Henceforth we state that the model vertical heating patterns, simulated by the embedded CRMs are biased. The heating needs to show a distinct difference between the two MISO modes so as to get a difference in their response in the circulation. As a consequence of the similar heating tendency profiles (Fig. 7a–c) the simulated divergence profile for the two ISO modes appear similar (note the similarity between the blue solid and dotted lines in Fig. 7d–f); contrary to observation (the

red solid and dotted lines in Fig. 7d–f differ). It appears that the barotropic and baroclinic modes are not properly simulated by the model. As the cloud processes and heating generated by them, is done by the CRM, this indicates that the CRM needs to be modified for proper representation of vertical heating distribution to capture the MISO modes. The reason the CRM can wrongly estimate the vigor of convective heating of strongly forced systems is probably because of the periodicity of the CRM domain, so that the convection resolved on CRM grid may effectively 'get stuck' in the same grid cell of the global model while in nature the convective system would eventually propagate out. This probably leads to persistent local precipitation biases in the Asian and Indian Monsoon regions in superparameterized framework (Khairoutdinov et al. 2005).

4 Conclusions

The above analyses are able to demonstrate that SP-CCSM has improved precipitation distribution and more importantly the model bias has improved as compared to its
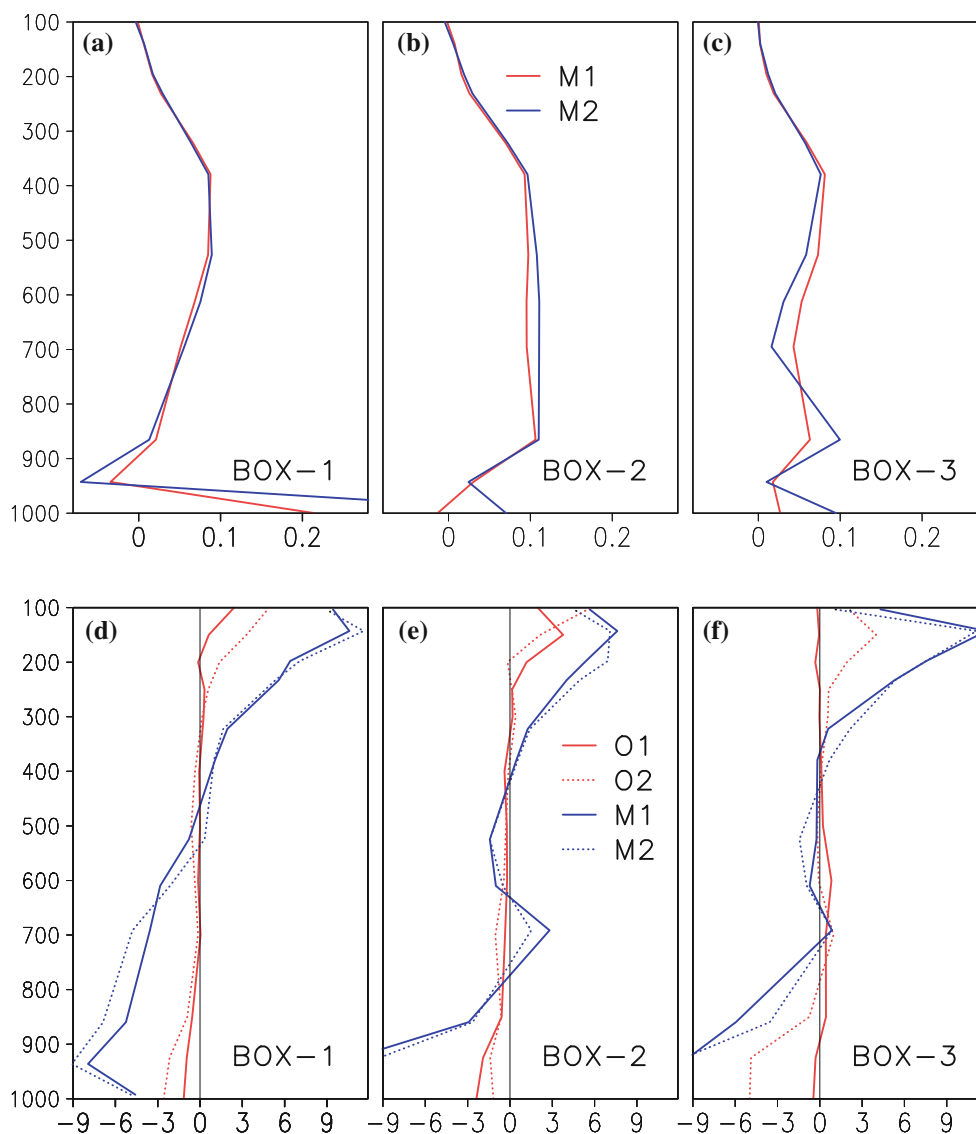
Fig. 7 Peak active monsoon composite of, (**a**–**c**) 15–30 (*red line*) and 35–80 (*blue line*) day filtered vertical heating tendency (10^{-4} K s^{-1}) of the CRM, in MMF; and (**d**–**f**) divergence profile (*red solid line* for O1-mode, *red dotted line* for O2-mode, *blue solid line* for M1-mode, *blue dotted line* for M2-mode), averaged over the *boxes* shown in Fig. 1b

superparameterized atmospheric counterpart. This means that the superparameterization in coupled model may become a useful tool for seasonal and intraseasonal forecast of ISM. However, on detailed analyses, some of the features of observed precipitation mode seem to have been simulated wrongly by the model. In fact, the simulated mode MISO-M1 is a model generated unique mode with no observational counterpart. In SP-CCSM the baroclinic component of MISO-M1 mode looks more prominent than the observation. The northward propagation caused by high frequency mode MISO-M1 along with the low frequency mode MISO-M2 further affirms the models inability to distinguish these two MISO modes. To find the reason

behind the prominent northward propagation by MISO-M1 mode and weak northward propagation by MISO-M2 mode, the components of the vorticity with respect to convection centre are analyzed. We demonstrate (Fig. 6f, h), that the unrealistic northward propagation in MISO-M1 (MISO-M2) is due to the fact that the anomalous barotropic vorticity lies to the north (south) of the convection centre unlike the observation. As the circulation is a consequence of heating, it seems that the vertical heating tendencies would play a key role in driving the bias of the model. The analyses and results further suggest that, mere coupling may not be enough; as it is related to the vertical profile of convective heating tendency generated by the CRMs,

which needs to be improved for a better simulation of the ISM and its intraseasonal oscillations.

References

Choudhury AD, Krishnan R (2011) Dynamical response of the South Asian Monsoon trough to latent heating from stratiform and convective precipitation. J Atmos Sci 68:1347–1363

Collins WD et al (2006) The community climate system model version 3 (CCSM3). J Clim 19:2122–2143

DeMott CA, Stan C, Randall DA, Kinter JL III, Khairoutdinov M (2011) The Asian monsoon in the superparameterized CCSM and its relationship to tropical wave activity. J Clim 24:5134–5156. doi:10.1175/2011JCLI4202.1

Duchon CE (1979) Lanczos filtering in one and two dimensions. J Appl Meteorol 18:1016–1022. doi:10.1175/1520-0450(1979

Goswami BN (2005) South Asian Summer Monsoon: An overview: in The Global Monsoon System: Research and Forecast Eds. C.-P. Chang, Bin Wang, Ngar-Cheung Gabriel Lau, Chapter 5, pp 47, WMO TD No. 1266, WMO, Geneva

Goswami BB, Mukhopadhyay P, Mahanta R, Goswami BN (2010) Multiscale interaction with topography and extreme rainfall events in the northeast Indian region. J Geophys Res 115:D12114. doi:10.1029/2009JD012275

Goswami BB, Mani NJ, Mukhopadhyay P, Waliser DE, Benedict JJ, Maloney ED, Khairoutdinov M, Goswami BN (2011) Monsoon intraseasonal oscillations as simulated by the superparameterized Community Atmosphere Model. J Geophys Res 116:D22104. doi:10.1029/2011JD015948

Grabowski WW (2001) Coupling cloud processes with the large-scale dynamics using the cloud-resolving convection parameterization (CRCP). J Atmos Sci 58:978–997

Guilyardi E, Braconnot P, Jin F–F, Kim ST, Kolasinski M, Li T, Musat I (2009) Atmosphere feedbacks during the ENSO in a coupled GCM with a modified atmospheric convection scheme. J Clim 22:5698–5718. doi:10.1175/2009JCLI2815.1

Hovmoller E (1949) Trough-and-ridge diagram. Tellus 1:62–66

Huffman GJ, Adler RF, Morrissey M, Bolvin DT, Curtis S, Joyce R, McGavock B, Susskind J (2001) Global precipitation at one-degree daily resolution from multi-satellite observations. J Hydrometeor 2:36–50. doi:10.1175/1525-7541(2001)002<0036: GPAODD>2.0.CO;2

Jiang X, Li T, Wang B (2004) Structures and mechanisms of the northward propagation boreal summer intraseasonal oscillation. J Clim 17:1022–1039. doi:10.1175/1520-0442(2004)017<1022: SAMOTN>2.0.CO;2

Kalnay E et al (1996) The NCEP/NCAR 40 year reanalysis project. Bull Am Meteorol Soc 77:437–471. doi:10.1175/1520-0477 (1996)077<0437:TNYRP>2.0.CO;2

Khairoutdinov M, Randall DA (2001) A cloud resolving model as a cloud parameterization in the NCAR community climate system model: preliminary results. Geophys Res Lett 28:3617–3620

Khairoutdinov M, Randall DA, DeMott CA (2005) Simulation of the atmospheric general circulation using a cloud-resolving model as super-parameterization of physical processes. J Atmos Sci 62:2136–2154

Liebmann B, Smith CA (1996) Description of a complete (Interpolated) outgoing longwave radiation dataset. Bull Am Meteorol Soc 77:1275–1277

Lin J-L, Weickman KM, Kiladis GN, Mapes BE, Schubert SD, Suarez MJ, Bacmeister JT, Lee M-I (2008) Subseasonal variability associated with Asian summer monsoon simulated by 14 IPCC AR4 coupled GCMs. J Clim 21:4541–4567. doi: 10.1175/2008JCLI1816.1

Piani C, Haerter JO, Coppola E (2010) Statistical bias correction for daily precipitation in regional climate models over Europe. Theor Appl Climatol 99:187–192

Randall DA et al. (2007) Climate models and their evaluation, in Climate Change 2007: The Physical Science Basis. Contribution of Working Group I to the Fourth Assessment Report of the Intergovernmental Panel on Climate Change, In S. Solomon et al. (ed), Cambridge Univ Press, Cambridge, UK, pp 589–662

Stan C, Khairoutdinov M, DeMott CA, Krishnamurthy V, Straus DM, Randall DA, Kinter JL III, Shukla J (2010) An ocean-atmosphere climate simulation with an embedded cloud resolving model. Geophys Res Lett 37:L01702. doi:10.1029/2009GL040822

Waliser DE et al (2003) AGCM simulations of intraseasonal variability associated with the Asian summer monsoon. Clim Dyn 21:423–446. doi:10.1007/s00382-003-0337-1

Wheeler M, Kiladis GN (1999) Convectively coupled equatorial waves: analysis of clouds and temperature in the wave number-frequency domain. J Atmos Sci 56:374–399. doi:10.1175/1520-0469(1999)056<0374:CCEWAO>2.0.CO;2

Wilks DS (1995) Statistical methods in the atmospheric sciences. Academic, San Diego